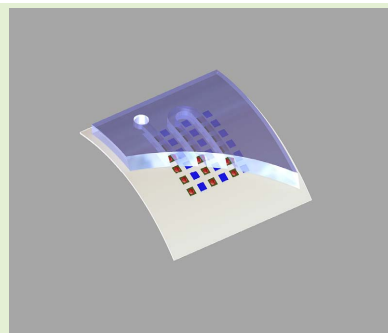


OLED-OPD Matrix for Sensing on a Single Flexible Substrate

Igor Titov, Markus Köpke, Nicole Christine Schneidewind, Janek Buhl, Yolande Murat, and Martina Gerken^{ID}, *Member, IEEE*

Abstract—Integration of organic light emitting diodes (OLEDs) and organic photodetectors (OPDs) on flexible plastic substrates promises compact and low-cost optical detection units for multiplex sensors. These units may be laminated to a microfluidic system for sensing applications in a liquid. Here, a 6×6 element matrix of alternating blue OLEDs and OPDs is demonstrated on a single flexible plastic substrate. The devices are fabricated by masked thermal evaporation on a $200 \mu\text{m}$ thick polyethylene terephthalate (PET) foil. The individual device size is $1 \text{ mm} \times 1 \text{ mm}$. Both OLEDs and OPDs are demonstrated to work. The spectral characteristics are shown to be suitable for fluorescence measurements. Signals from fluorescence-labeled spots above the OPDs under OLED excitation are investigated. Successful operation of the OLED-OPD matrix for reflection measurement is demonstrated.

Index Terms—OLED, OPD, flexible, sensor, fluorescence.



I. INTRODUCTION

FLEXIBLE and on-skin wearable sensors are highly promising for continuous health monitoring [1]. Lochner *et al.* proposed the realization of a pulse oximeter based on two types of OLEDs and OPDs on a single flexible substrate for a wearable oxygen sensor [2]. They demonstrated the device concept with OLEDs fabricated on separate rigid substrates. Mayr *et al.* presented an array of OPDs on a flexible substrate illuminated by an OLED on a separate substrate [3]. Liu *et al.* discussed different configurations of all-organic sensors for simultaneous oxygen and pH monitoring; OLEDs integrated with sensing films on rigid substrates and OPDs on separate substrates [4]. Yokota *et al.* presented an oximeter with two different OLEDs and an OPD by lamination of ultraflexible foils with different types of OLEDs and OPDs [5]. These foils were obtained by release from a sacrificial layer and each

foil has only one type of optoelectronic device on it. While very impressive results are achieved with the lamination of several ultraflexible substrates, this procedure is not easily upscaled for the parallel fabrication of many sensor units. We have previously demonstrated the integration of OLEDs and OPDs on single rigid substrates in a monolithic integration approach [6] and proposed a device configuration for fluorescence measurements [7].

Our long-term goal is the realization of a small, multiplexed sensor for point-of-need analysis. For example, for testing five different parameters of interest with threefold redundancy and three reference sites, 18 simultaneous measurements need to be integrated on a chip. In the past we demonstrated a hand-held camera system for multiplex detection [16]. This approach combined a camera readout system with a disposable chip. An even more compact approach is proposed here based on hybrid integration of the optical readout system with the microfluidic system. For biosensing the surface may be functionalized with capture molecules for the binding of specific fluorescence-labelled biomaterial. Such an integrated approach would require only an electrical (or wireless) connection and could be read out, e.g., with a smartphone. All sensing elements are permanently aligned allowing a high degree of miniaturization. Using flexible plastic materials furthermore promises cost-effective, large-scale fabrication and rugged systems. The key element for the hybrid integration is an optoelectronic system providing 18 detection sites. Excluding movable parts this corresponds to 18 photodetectors –

Manuscript received March 10, 2020; accepted March 30, 2020. Date of publication April 6, 2020; date of current version June 18, 2020. This work was supported in part by Interreg under Project RollFlex 1_11.12.2014 and in part by Zentrales Innovationsprogramm Mittelstand (ZIM) (Project AuToilette) under Grant ZF4558802RH8. This is an expanded paper from the 2019 IEEE International Conference on Flexible and Printable Sensors and Systems (FLEPS) [14]. The associate editor coordinating the review of this article and approving it for publication was Prof. Ravinder S. Dahiya. (*Corresponding author: Igor Titov.*)

The authors are with the Chair for Integrated Systems and Photonics, Institute of Electrical Engineering and Information Technology, Kiel University, 24143 Kiel, Germany (e-mail: igti@tf.uni-kiel.de).

Digital Object Identifier 10.1109/JSEN.2020.2986051

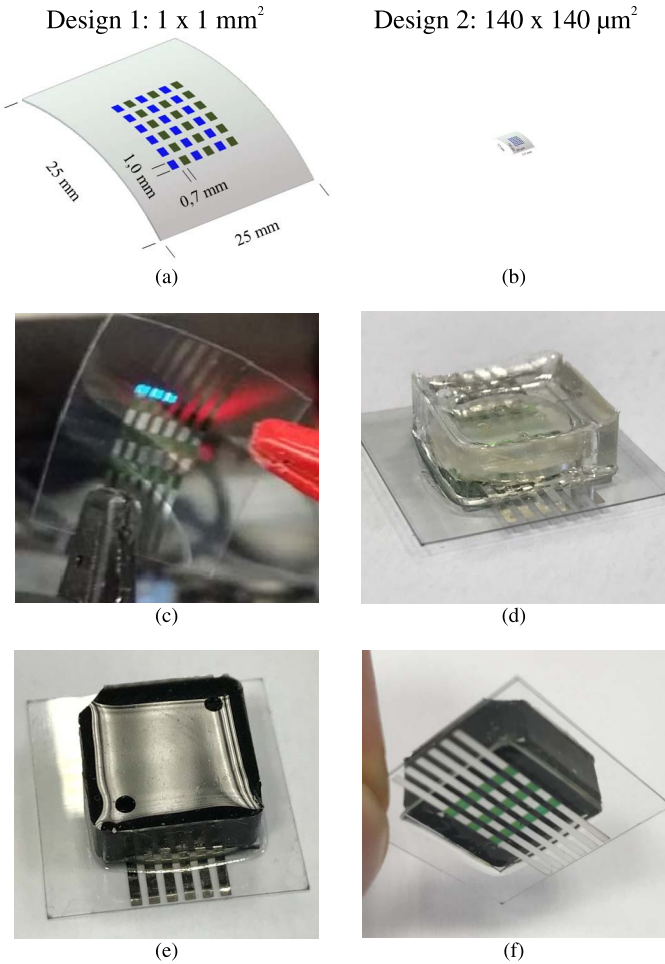


Fig. 1. (a) Design 1: Matrix layout with 18 OLEDs (blue) and 18 OPDs (green) on a 200- μm thick, $2.5 \times 2.5 \text{ cm}^2$ PET foil. Device sizes are $1 \times 1 \text{ mm}^2$. (b) Design 2: 18 OLEDs (blue) and 18 OPDs (green) with device sizes $140 \times 140 \mu\text{m}^2$ on a 200- μm thick PET foil. (c) Photograph of fabricated design 1. (d) Matrix of design 1 with microfluidic chamber in transparent PDMS. Holes for inlet and outlet are visible. (e,f) Matrix of design 1 with microfluidic chamber in black PDMS for stray light suppression.

one covering each detection site. Here, we investigate the realization of a matrix of 18 OPDs and 18 OLEDs as excitation sources on a single flexible substrate. Using pairs of OPDs and OLEDs allows for a flat, monolithically integrated design.

In section II we present ray tracing simulations for two different OLED-OPD matrix designs as shown in Fig. 1. Design 1 uses 36 devices of size $1 \text{ mm} \times 1 \text{ mm}$ and design 2 has 36 devices of size $140 \mu\text{m} \times 140 \mu\text{m}$. In both designs a 200- μm thick PET foil is used. For both designs the case of a transparent microfluidic system is compared to the case of a black microfluidic system. The system efficiency for fluorescence sensing is calculated for the different designs. Section III presents the fabrication procedure for design 1. The experimental characterization of the OPD and OLED devices is given in section IV. Furthermore, section IV presents first fluorescence experiments. For these experiments we employ the oxygen sensitive dye $\text{Ru}(\text{bpy})_3\text{Cl}_2$, which is

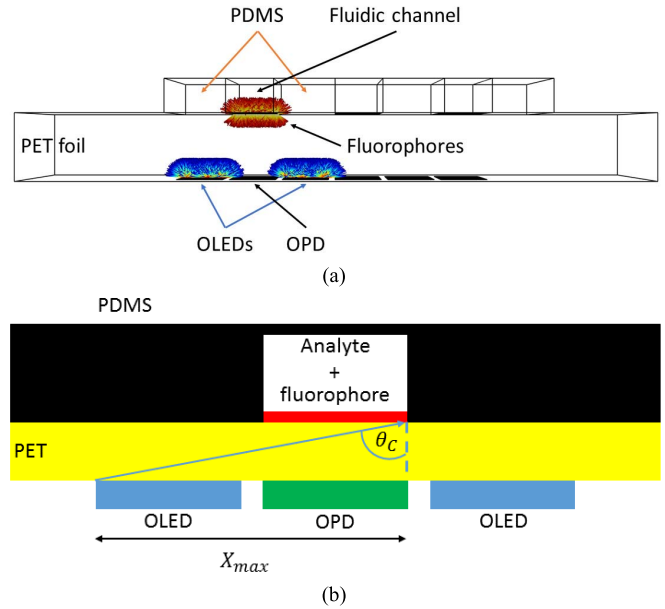


Fig. 2. Model for ray-tracing simulations. (a) Matrix of OLEDs emitting into the substrate and OPDs on PET foil. Fluorescence spots are above OPDs on the other side of the PET foil. A PDMS microfluidic chip is placed such that the fluidic channels are above the OPDs. The PDMS fluidic channels are placed above the fluorophore arrays. (b) 2D view of system with black PDMS microfluidics to prevent stray light.

used commonly to detect dissolved oxygen by fluorescence quenching [9]. Conclusions are given in section V.

II. FLUORESCENCE SENSOR SIMULATIONS

First, we conduct raytracing simulations in order to estimate the system efficiency for fluorescence sensing. As shown in Fig. 2 OLEDs are assumed to be emitting into the substrate and OPDs are sensitive to light incident from the substrate side. In the hybrid integration approach the PDMS microfluidic is assumed to be placed on the opposite side of the PET foil from the active organic optoelectronics. This ensures that a controlled optical path is achieved and no damage to the devices due to the liquid is expected. The fluidic channels are considered to be located above the row of OPDs. The fluorophores generating the signal are located above the OPD and the active region has the same size as the OPD. We choose this alignment to achieve the highest fluorescence intensity.

A. Simulation Model

In the ray-tracing simulation model, we do not model the full OLED and OPD stack. Instead we assume that the OLEDs emit from a transparent conductive indium tin oxide (ITO) layer with an emission power density of 1750 W/m^2 . The OPDs are considered as absorptive surfaces. The microfluidic system is modelled by a $100 \mu\text{m}$ thick polydimethylsiloxane (PDMS) cap with channels to transport the water-based analyte. The channels have the same width as the OPDs. We consider microfluidics fabricated from transparent and black PDMS. Table I summarizes the refractive indices used in the simulation. The emission vacuum wavelength is set

TABLE I
OPTICAL PROPERTIES USED FOR THE SIMULATION

Medium	Refractive index	Source
ITO	1.9858	[11]
H ₂ O	1.3376	[12]
PET	1.6	[13]
PDMS	1.4425	[10]

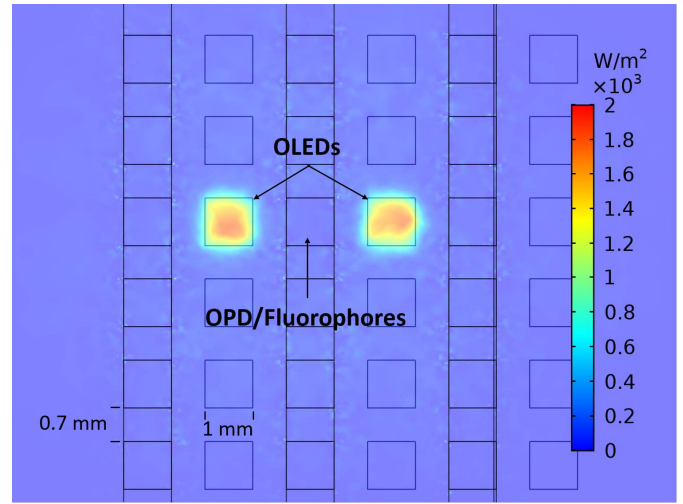
to 450 nm. We assume a Lambertian emission pattern for each individual OLED and assume that the detection region is excited by two neighboring OLEDs. The simulations are carried out with the Ray Optics Module in COMSOL Multiphysics®. The number of rays per release was set to 10^3 with 10^3 rays in wave vector space.

B. Simulation Results

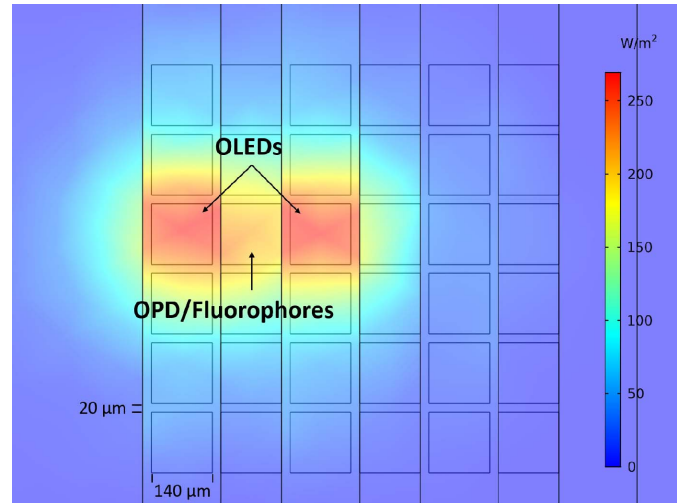
First the irradiation profile of the top surface of the PET foil by the OLEDs is considered. This surface is defined as a cut-plane for accumulating irradiation power in the ray-tracing software. Figs. 3(a,b) show the simulated emission power density for two operational OLEDs for design 1 and design 2, respectively. We use the same radiosity for the small devices as for the large devices. The radiosity of the small OLEDs is kept at 1750 W/m^2 . If a larger active area is desired, stripes of active devices should be used. Note that the radiosity of the OLED is transferred to the top surface of the PET foil above the OLED for design 1 as the device size is significantly larger than the PET-foil thickness. For design 2 with $140 \mu\text{m} \times 140 \mu\text{m}$ OLEDs the light is already spread to a larger area with a reduced irradiance at the top side of the $200\text{-}\mu\text{m}$ thick PET foil above the OLED.

At the position of the fluorescence region above the OPDs only a small irradiance is found. The average irradiance on the sensitive spot is obtained by defining the fluorophores as an accumulator. An average irradiance of 43 W/m^2 is simulated at the location of the fluorophores for design 1. The average irradiance at the position of the fluorophores is increased to 228 W/m^2 for design 2, which is ~ 5 times higher than obtained from $1 \text{ mm} \times 1 \text{ mm}$ devices even though the absolute emitted power of the smaller devices is ~ 50 times lower. Fig. 3(c) depicts a selection of rays showing that still only a relatively small fraction of rays reaches the illumination area of interest.

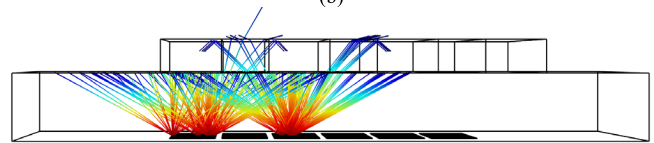
Next, we consider how much of the emitted fluorescence reaches the detector. Here, we consider the oxygen sensitive dye $\text{Ru}(\text{bpy})_3\text{Cl}_2$ as an example. Suzuki *et al.* measured the absolute quantum yield Φ_p for this ruthenium complex at 298K to be 0.063 (in deaerated water) [8]. We used the results obtained from the simulation shown in Fig. 3(a,b) to calculate the emitted fluorescent light after the excitation of the fluorophore. For design 1 the average irradiation of 43 W/m^2 of the dye corresponds to a fluorescence radiosity of $\sim 2 \text{ W/m}^2$ for the given quantum yield and considering the wavelength shift from 450 nm to 615 nm. For design 2 the average irradiation of 228 W/m^2 of the dye corresponds to a fluorescence radiosity of $\sim 10.5 \text{ W/m}^2$. To investigate



(a)



(b)



(c)

Fig. 3. (a) Surface distribution of the $1 \text{ mm} \times 1 \text{ mm}$ OLED radiosity of 1750 W/m^2 on PET-foil. (b) Surface distribution of the $140 \mu\text{m} \times 140 \mu\text{m}$ OLED radiosity of 1750 W/m^2 on PET-foil. (c) Side view of $140 \mu\text{m} \times 140 \mu\text{m}$ active device matrix with small selection of rays.

the amount of detected emission on the OPD, we defined the fluorophore as a spherical ray release device with a source radiance of 10.5 W/m^2 and the OPD as an accumulator. This results in an average irradiance of 0.48 W/m^2 on the $140 \mu\text{m} \times 140 \mu\text{m}$ OPD device equaling a received power of $\sim 9.5 \text{ nW}$. For design 1 the average irradiance is calculated to be $\sim 1 \text{ W/m}^2$. The system efficiency from OLED radiosity in W/m^2 to OPD irradiance in W/m^2 is 0.6% for design 1 and 0.3% for design 2, respectively.

Due to the better system efficiency as well as due to less stringent fabrication requirements, we fabricated design 1.

TABLE II
EFFICIENCY ANALYSIS

	Design 1: 1 x 1 mm ² devices; transparent PDMS	Design 1: 1 x 1 mm ² devices; black PDMS	Design 2: 140 x 140 μm ² devices; transparent PDMS	Design 2: 140 x 140 μm ² devices; black PDMS
OLED emission power density J_{OLED}	1750 W/m ²	1750 W/m ²	1750 W/m ²	1750 W/m ²
Fluorophore area	1 x 1 mm ²	1 x 1 mm ²	140 x 140 μm ²	140 x 140 μm ²
Fluorophore illumination avg.	43 W/m ²	43 W/m ²	228 W/m ²	228 W/m ²
Fluorophore quantum efficiency	6.3%	6.3%	6.3%	6.3%
Fluorescence on OPD E_{OPD}	1 W/m ²	1 W/m ²	0.5 W/m ²	0.5 W/m ²
System efficiency $\eta = E_{OPD}/J_{OLED}$	0.6 ‰	0.6 ‰	0.3 ‰	0.3 ‰
Stray light on OPD	1.8%	0.05%	~0%	~0%

Before continuing to the experimental results, we want to use the ray tracing simulations to consider the stray light from OLED to OPD for the two different designs. This is background light in the experiment.

The OLED stray light on the OPD is simulated by defining the OPD between two OLEDs as a ray detector. This function counts the incident rays, which are reflected by interfaces. For the design 1 and transparent PDMS, we obtained a value of 1.8%, i.e., 1.8% of the total number of released rays is directly detected on the OPD. In contrast, for device 1 and black PDMS, modeled as perfect absorber, we observe a reduction to 0.05%.

In design 2 we chose the lateral dimension X_{max} of one OLED-OPD pair in Fig. 2(b) such that the ray shown is just at the critical angle for total internal reflection θ_C . Thus, light guided by total internal reflection does not reach the OPD in this design. All other rays directly incident from the OLED onto the fluorophore have a smaller angle. For the interface between water with a refractive index $n_{H_2O} = 1.3376$ and PET with $n_{PET} = 1.6$ we obtain $\theta_C \approx 57^\circ$. For a PET-foil thickness of 200 μm this gives us a value of $X_{max} \approx 300 \mu\text{m}$. Consequently, the individual device size was set to 140 μm × 140 μm with a distance of 20 μm between devices.

Due to the close positioning of OLEDs and OPDs, stray light is effectively suppressed for design 2 and is 0% within the simulation assumptions. The simulation results are summarized in Table II.

III. OLED-OPD MATRIX FABRICATION

Fig. 1 depicts the matrix layout of design 1, which we fabricated. The OLED and OPD layer sequences are given in Fig. 4. We realized 18 OLEDs and 18 OPDs with an active area of 1 × 1 mm² each on one substrate. The OLED-OPD matrix is fabricated on a 25 × 25 mm² polyethylene terephthalate (PET) foil with a thickness of 200 μm and with an indium tin oxide (ITO) top layer of 20 nm (EMI Tape Co., Thorlabs).

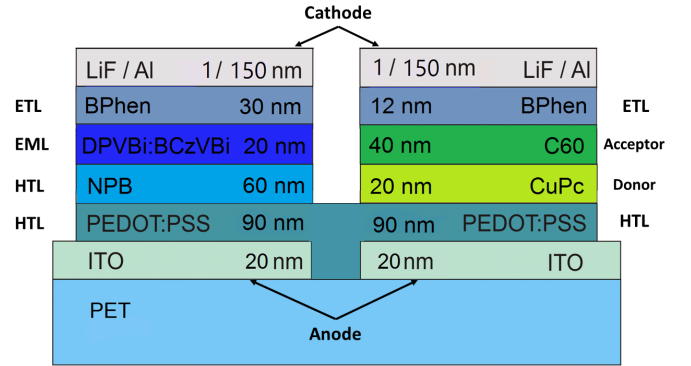


Fig. 4. Schematic diagram of OLED stack (left) and OPD stack (right) on a single PET substrate. The function of the layers is as follows: ETL: electron transport layer, EML: emission layer, HTL: hole transport layer.

Via ultraviolet (UV) lithography and wet etching, the ITO layer is structured to form transparent anode contact pads. For this purpose, the PET coated with ITO is cleaned first in acetone and then in isopropanol in an ultrasonic bath for 10 minutes, each. After dehydrating the sample for 15 minutes at 90°C on a hotplate, the photoresist (AZ1518, MicroChemicals) is spin coated at 2850 rpm for 30 seconds. Then a soft bake for 60 seconds at 90°C on a hotplate is performed. After UV exposure and resist development (60 seconds with developer AZ726 MIF, MicroChemicals, stopped with deionized (DI) water) the resist is hardened at 115°C for 60 seconds. To remove the excess ITO and form the ITO anode pads the sample is etched with 30% hydrochloric acid for 2 minutes. Next, the resist is stripped off the sample by using acetone for 2 minutes and isopropanol for 10 minutes in an ultrasonic bath.

Before the first organic layers for the OLEDs and OPDs are processed the samples are dehydrated for 12 hours at 90°C and treated with oxygen plasma (2 minutes, 8 sccm O₂ and 100 W RF power) such that the surface becomes hydrophilic for better adhesion of the organic layers.

First an organic 90 nm thin layer of poly(3,4-ethylenedioxy thiophene):polystyrene sulfonate (PEDOT:PSS, Sigma-Aldrich Chemie GmbH) is deposited by wet-process using the spin-coating technique (3500 rpm, 30 s) on top of the anode. Following this common step for both OLEDs and OPDs, the remaining organic layers on top of the PEDOT:PSS are evaporated using a thermal evaporation system.

The OLED layer structure is as follows: a layer of 60 nm of N,N'-Bis(naphthalene-1-yl)-N,N'-bis(phenyl) benzidine (NPB) as hole transport layer (HTL), then for the emission layer a 20 nm of 4,4'-Bis(2,2-diphenylvinyl)-1,1'-biphenyl (DPVBi) doped with 5% of 4,4'-Bis(9-ethyl-3-carbazovinylen)-1,1'-biphenyl (BCzVBi) to generate a narrowband emission spectrum in the blue spectral range. For the combined electron transport layer (ETL) and hole blocking layer (HBL) a 30 nm layer of 4,4'-Bis(9-ethyl-3-carbazovinylen)-1,1'-biphenyl (BPhen) is deposited, followed by cathode pads consisting of 1 nm lithium fluoride (LiF) and 150 nm aluminum (Al).

The OPD layer structure on the PEDOT:PSS starts with an electron donor layer of 20 nm Copper(II) phthalocyanine (CuPc), then an electron acceptor layer of 40 nm C60, followed by 12 nm BPhen (ETL). The cathode pads have the same layer structure as for the OLED. Fig. 2(c) shows a photograph of a fabricated device matrix operated with a 9 V battery.

For the microfluidic system we suggest to employ a black flexible polymer for the suppression of stray light. We fabricated microfluidic chambers by molding polydimethylsiloxane (PDMS) mixed with Carbon Black (Ketjenblack®EC-600JD, Akzo Nobel Polymer Chemicals B.V.) from a Teflon mold. These systems are still rather bulky as shown in Fig. 1(e,f), but may be further miniaturized.

IV. EXPERIMENTAL CHARACTERIZATION

A. Single-Device Characterization

To prevent degradation of the organic materials during the characterization in the oxygen environment the OLED-OPD matrix was encapsulated with glass and placed in a darkened environment. Characterization is performed without the microfluidic chamber. Two Source Measure Units (SMUs) are used for electrical characterization. The I-V characteristic of the OLED fabricated on PET foil is shown in Fig. 5(a). The emission area of the OLED is aligned above a S1223-01 photodiode (Hamamatsu Photonics K.K.) to obtain the relative light output at different operating voltages. For comparison the I-V curve for an OLED on glass with the same layer stack, but 130 nm ITO anode is plotted as well. The OLEDs fabricated on PET foil show a higher onset voltage and a poorer luminous efficiency. This is attributed to the series resistance of the thin 20 nm ITO layer.

The OPD device characteristics are shown in Fig. 5(b). The I-V curves of two sample OPDs – one on PET and one on glass – are measured under dark conditions and illumination by a red LED operated at 2.5 V and 20 mA (10560 mcd, LL-503VC2E-V1-4DC, Lucky Light Electronics Co., Ltd). The OPD on PET (blue) and on glass (red) show typical

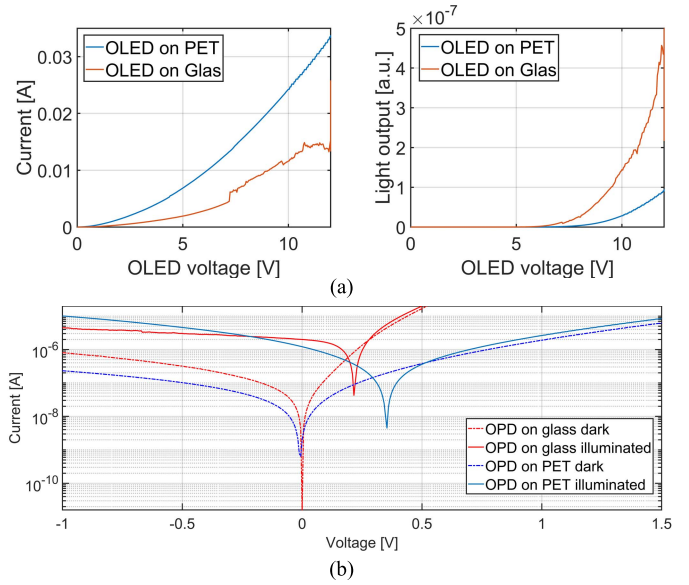


Fig. 5. (a) I-V curve (left) and the light output with voltage (right) for an OLED fabricated on glass (orange) and an OLED fabricated on PET (blue). (b) I-V characteristic of the OPDs fabricated on PET and glass in the dark and under illumination.

diode characteristics. The open-circuit voltage and the short-circuit current under illumination were observed to be 354 mV and $-1.21 \mu\text{A}$ for PET and 216 mV and $-2 \mu\text{A}$ for glass, respectively. The I-V curves show that the light conversion efficiency of the glass device is higher than on PET foil. More details on the device behavior were presented in [17] and [18].

B. OLED-OPD-Pair Characterization

Using a simple matrix electrode design leads to leakage currents when operating OLEDs and OPDs simultaneously. Thus, we fabricated a second-generation matrix with an electrode design galvanically separating neighboring OLED and OPD devices. In Fig. 6(a) we plot the OPD short circuit photocurrent for rectangular pulse operation of the neighboring OLED at 15 V, 1.2 mA and 0.25 Hz. This measurement was carried out in dark environment without the black PDMS chamber presented in Fig. 1(e,f). The switching behavior is clearly observed and reproduced without showing degradation of the organic materials. The light from the OLED reaching the OPD through the common substrate induces an absolute photocurrent at $\sim 3.9 \text{ nA}$. This is the stray light discussed in section II. The OPD dark current amounts to $\sim 0.25 \text{ nA}$. Fig. 6(b) shows the direct light of the OLED on the OPD while manually reflecting OLED light to the OPD with an optical mirror. In this experiment, the OLED was operated continuously at 10 V. The absolute value of the background current was observed to be $\sim 0.95 \text{ nA}$. The OPD photocurrent increases to $\sim 7.2 \text{ nA}$ by maximizing the reflection of direct light. These experiments show the successful linking of OLED and OPD.

C. Fluorescence Sensing

As the test case for fluorescence sensing we consider the fluorophore $\text{Ru}(\text{dpp})_2\text{Cl}_3$, which is widely used for

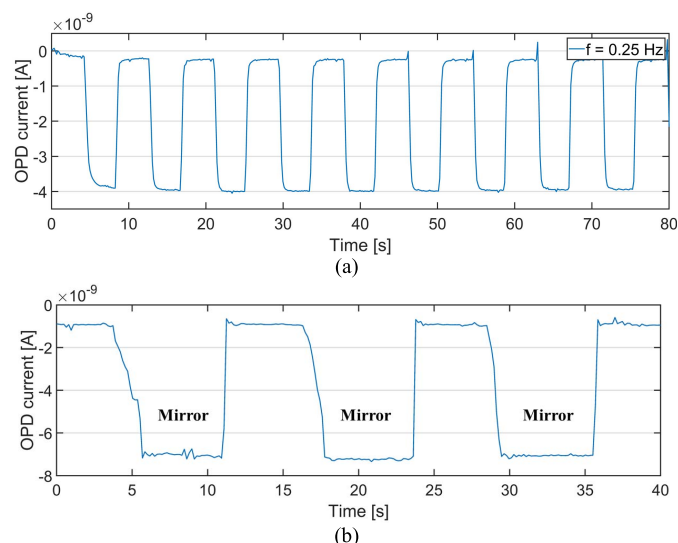


Fig. 6. (a) OPD on PET short circuit photocurrent for rectangular pulse modulated OLED at 15 V, 1.2 mA and 0.25 Hz. (b) Enhancement of OPD signal by manual reflection of direct OLED light onto the OPD with a silver mirror. The OLED is operated continuously at 10 V.

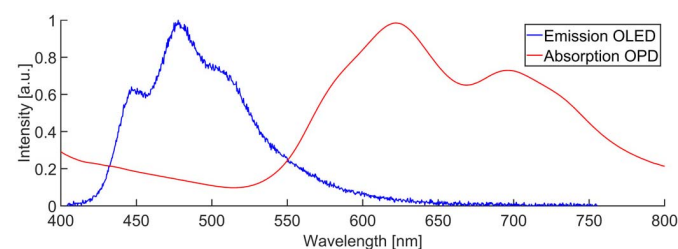


Fig. 7. Normalized emission spectrum of the OLED and absorption spectrum of the OPD.

dissolved-oxygen sensing [15]. The absorption and the emission maxima are located at 450 nm and 620 nm, respectively. Fig. 7 shows the absorption spectrum of the OPD layer stack and the emission spectrum of the OLED layer stack. The devices used for this characterization were fabricated on separate glass substrates for spectral analysis. The spectral characteristic demonstrates that the peaks are suitably located for excitation and fluorescence detection of $\text{Ru}(\text{dpp})_2\text{Cl}_3$. An additional optical filter in front of the OPD is necessary to obtain the necessary suppression of the excitation light in fluorescence measurements. This filter may either be included on the substrate foil or integrated in the OPD design.

Next, we coated a PET foil with $\text{Ru}(\text{dpp})_2\text{Cl}_3$. The immobilization was performed in methyltriethoxysilane (MTEOS, Sigma-Aldrich Chemie GmbH, Germany) by the sol-gel process presented in [15]. The chemicals were analytical grade and used as received. Placing this $\text{Ru}(\text{dpp})_2\text{Cl}_3$ -coated PET foil on top of the OLED-OPD matrix we measure the OLED spectrum through the $\text{Ru}(\text{dpp})_2\text{Cl}_3$ -coated PET foil with a fiber-coupled spectrometer. An optical 560 nm longpass filter (O-56, Edmund Optics, Inc.) is included in front of the spectrometer to filter direct OLED light.

Fig. 8(a) shows the difference spectrum of the $\text{Ru}(\text{dpp})_2\text{Cl}_3$ -coated PET foil. In the inset, we plot the original data

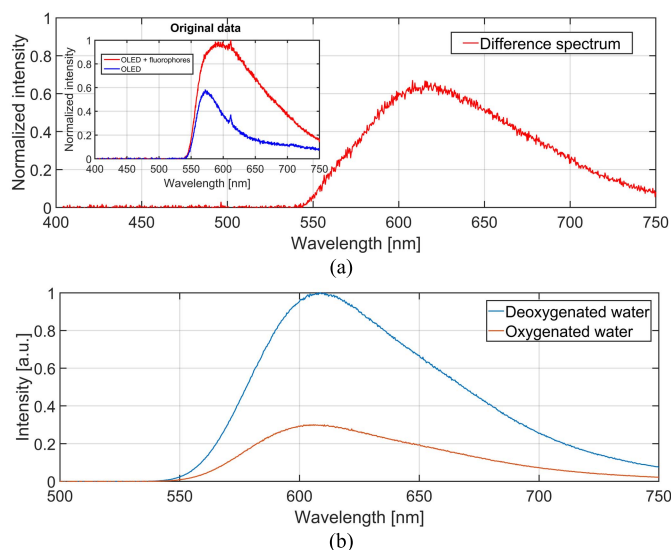


Fig. 8. (a) Difference spectral characteristics of the emission of a $\text{Ru}(\text{dpp})_2\text{Cl}_3$ -coated PET foil excited by the OLED (560-nm long-pass filter employed in both measurements). Inset: Measured data used for differencing. (b) For comparison: Emission characteristic of $\text{Ru}(\text{dpp})_2\text{Cl}_3$ from a dissolved oxygen quenching measurement carried out with a blue LED.

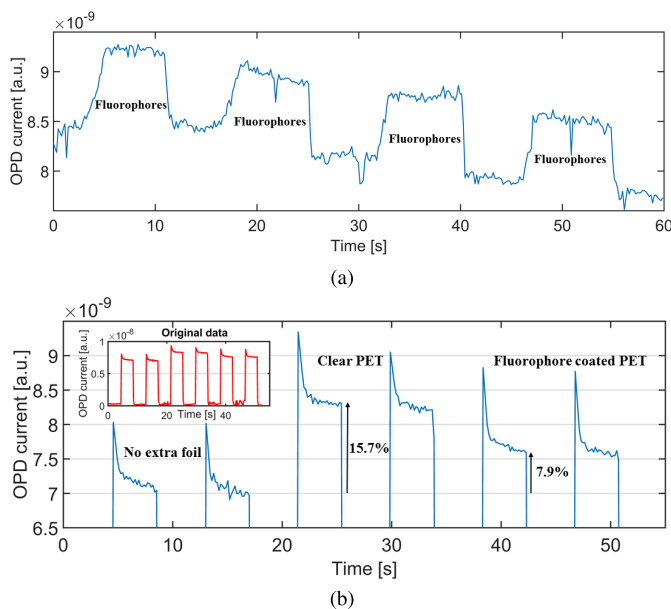


Fig. 9. (a) Enhancement of the photocurrent by adding a $\text{Ru}(\text{dpp})_2\text{Cl}_3$ -coated PET foil on top of the OLED-OPD matrix. (b) Signal comparison between a clear PET foil and a $\text{Ru}(\text{dpp})_2\text{Cl}_3$ -coated PET foil.

normalized at the emission peak with $\text{Ru}(\text{dpp})_2\text{Cl}_3$ -coated PET foil (red curve). The difference of the signals shows a maximum, which fits to the expected emission of $\text{Ru}(\text{dpp})_2\text{Cl}_3$ shown in Fig. 8(b).

In Fig. 9(a) we present a measurement of an OLED-OPD matrix fabricated on PET foil, which shows the OPD photocurrent with a continuously operated neighboring OLED at 15 V and ~ 3.5 mA. The increase of the photocurrent was achieved by adding and removing the $\text{Ru}(\text{dpp})_2\text{Cl}_3$ coated PET foil on top of the operated matrix.

In order to investigate if the OPD current increase is due to a fluorescence effect or due to increased reflection off the

substrate, we conducted a second type of experiment (using a new matrix as the old one was degraded). We operate the OLED with a rectangular pulse at 20 V and ~ 2.25 mA to have a clear base line. Then we place a non-coated PET foil above the matrix and finally exchange this with the Ru(dpp)₂Cl₃ coated PET foil. Fig. 9(b) shows the resulting OPD photocurrent for two pulses in each of the three conditions – no extra PET foil, non-coated PET foil, and Ru(dpp)₂Cl₃ coated PET foil. The first two peaks are caused by stray light from the OLED to the OPD resulting in an OPD current of ~ 7 nA. The second pair of peaks are caused by reflection off the non-coated PET foil superimposed on the stray light yielding an OPD current of ~ 8.3 nA. The last pair of peaks shows the superposition of stray light, reflectance and the fluorophore effect of the Ru(dpp)₂Cl₃ coated PET foil. The signals decrease to ~ 7.6 nA in comparison to clear PET. Thus, we conclude that absorption effects of the fluorophore reducing the signal dominate fluorescence effects increasing it. This result shows that for successful fluorescence sensing OPDs with a narrowband absorption around the fluorescence or a longpass filter for direct light suppression need to be used. On the other hand, the experiments also clearly demonstrate that the OLED-OPD matrix detection unit is functional and may be used for sensing tasks requiring the measurement of a change in direct light reflection, e.g. absorption or refractive index measurements.

V. CONCLUSIONS

In conclusion, we demonstrated the monolithic integration of a matrix of 18 OLEDs and 18 OPDs on a flexible substrate. Operation of both device types as well as detection of OLED light with the OPD was demonstrated. It was found that electric matrix operation of OLEDs and OPDs leads to leakage currents between the two device types due to the highly different operating voltages. Galvanic separation of OLEDs and OPDs on a single substrate prevents such leakage currents. The lifetime of the devices was short, hence they were characterized encapsulated with glass. This prevents degradation of the organic layers upon oxygen contact. For flexible applications the substrates can be encapsulated with an additional foil on top of the active devices.

The spectra of the designed devices have suitable peak positions for fluorescence measurements. We demonstrated the excitation of the oxygen sensitive fluorophore Ru(dpp)₂Cl₃ with the OLED. The fluorescence light was observed with a spectrometer. The OPD detects a superposition of direct light effected by fluorophore absorption and the fluorescence signal. Our experiments suggest that the absorption effect is dominating in the current system. Thus, OPDs with a narrowband absorption around the fluorescence are preferable. Alternatively, a longpass filter needs to be integrated.

For suppressing stray light from the OLED to the OPD we suggest the use of smaller device sizes. Design 2 is also preferable for a smaller overall system size.

The demonstrated flexible OLED-OPD matrix serves as a platform technology for new multiplex sensor concepts based on optoelectronic measurements. It is ready to use for absorption or refractive index measurements changing the intensity of reflected light.

REFERENCES

- [1] Kenry, J. C. Yeo, and C. T. Lim, "Emerging flexible and wearable physical sensing platforms for healthcare and biomedical applications," *Microsyst. Nanoeng.*, vol. 2, no. 1, Dec. 2016, Art. no. 16043.
- [2] C. M. Lochner, Y. Khan, A. Pierre, and A. C. Arias, "All-organic optoelectronic sensor for pulse oximetry," *Nature Commun.*, vol. 5, no. 1, pp. 1–7, Dec. 2014.
- [3] T. Mayr *et al.*, "An optical sensor array on a flexible substrate with integrated organic opto-electric devices," *Procedia Eng.*, vol. 5, pp. 1005–1008, Jun. 2010.
- [4] R. Liu, T. Xiao, W. Cui, J. Shinar, and R. Shinar, "Multiple approaches for enhancing all-organic electronics photoluminescent sensors: Simultaneous oxygen and pH monitoring," *Analytica Chim. Acta*, vol. 778, pp. 70–78, May 2013.
- [5] T. Yokota *et al.*, "Ultraflexible organic photonic skin," *Sci. Adv.*, vol. 2, no. 4, Apr. 2016, Art. no. e1501856, doi: [10.1126/sciadv.1501856](https://doi.org/10.1126/sciadv.1501856).
- [6] D. Threm, J. L. Gugat, A. Pradana, M. Radler, J. Mikat, and M. Gerken, "Self-aligned integration of spin-coated organic light-emitting diodes and photodetectors on a single substrate," *IEEE Photon. Technol. Lett.*, vol. 24, no. 11, pp. 912–914, Jun. 2012.
- [7] S. Jahns, A. F. K. Iwers, J. Balke, and M. Gerken, "Organic optoelectronics for lab-on-chip fluorescence detection," *Technisches Messen*, vol. 84, no. s1, pp. 48–51, Sep. 2017.
- [8] K. Suzuki *et al.*, "Reevaluation of absolute luminescence quantum yields of standard solutions using a spectrometer with an integrating sphere and a back-thinned CCD detector," *Phys. Chem. Chem. Phys.*, vol. 11, no. 42, pp. 9850–9860, 2009.
- [9] X. Xiong, Y. Tang, and B. Zheng, "Dissolved oxygen sensor based on sol-gel matrix doped with tris(2,2'-bipyridine)ruthenium dichloride," *J. Chongqing Univ.*, vol. 12, no. 1, pp. 11–15, 2013.
- [10] F. Schneider, J. Draheim, R. Kamberger, and U. Wallrabe, "Process and material properties of polydimethylsiloxane (PDMS) for optical MEMS," *Sens. Actuators A, Phys.*, vol. 151, no. 2, pp. 95–99, Apr. 2009.
- [11] T. A. F. König *et al.*, "Electrically tunable plasmonic behavior of Nanocube—Polymer nanomaterials induced by a redox-active electrochromic polymer," *ACS Nano*, vol. 8, no. 6, pp. 6182–6192, Jun. 2014.
- [12] G. M. Hale and M. R. Querry, "Optical constants of water in the 200-nm to 200- μ m wavelength region," *Appl. Opt.*, vol. 12, no. 3, p. 555, Mar. 1973.
- [13] M. Biron, "Plastics solutions for practical problems," in *Thermoplastics Thermoplastic Composites*, 2nd ed. New York, NY, USA: William Andrew, 2013, pp. 831–984.
- [14] N. Schneidewind, M. Kopke, J. Buhl, Y. Murat, and M. Gerken, "OLED-OPD matrix for fluorescence sensing on a single flexible substrate," in *Proc. IEEE Int. Conf. Flexible Printable Sensors Syst. (FLEPS)*, Glasgow, U.K., Jul. 2019, pp. 1–3.
- [15] C. McDonagh, P. Bowe, K. Mongey, and B. D. MacCraith, "Characterisation of porosity and sensor response times of sol-gel-derived thin films for oxygen sensor applications," *J. Non-Crystalline Solids*, vol. 306, no. 2, pp. 138–148, 2002.
- [16] S. Jahns *et al.*, "Handheld imaging photonic crystal biosensor for multiplexed, label-free protein detection," *Biomed. Opt. Express*, vol. 6, no. 10, p. 3724, Oct. 2015, doi: [10.1364/boe.6.003724](https://doi.org/10.1364/boe.6.003724).
- [17] T.-G. Kim, H.-S. Oh, Y.-H. Kim, and W.-Y. Kim, "Study of deep blue organic light-emitting diodes using doped BCzVBi with various blue host materials," *Trans. Electr. Electron. Mater.*, vol. 11, no. 2, pp. 85–88, Apr. 2010, doi: [10.4313/teem.2010.11.2.085](https://doi.org/10.4313/teem.2010.11.2.085).
- [18] P. Peumans and S. R. Forrest, "Very-high-efficiency double-heterostructure copper phthalocyanine/C60 photovoltaic cells," *Appl. Phys. Lett.*, vol. 79, no. 1, pp. 126–128, Jul. 2001, doi: [10.1063/1.1384001](https://doi.org/10.1063/1.1384001).



Igor Titov was born in Kazakhstan in 1991. He received the master's degree in electrical engineering and information technology from Kiel University, Germany, in 2018, where he is currently pursuing the Ph.D. degree with the Chair for Integrated Systems and Photonics, Institute of Electrical Engineering and Information Technology. His research interests include biosensors and lab-on-a-chip systems.



Janek Buhl was born in Kiel, Germany, in 1990. He received the B.S. and M.S. degrees in electrical engineering, information technology and business management and the second B.S. degree in chemistry and business management from Kiel University, Germany, in 2017. He is currently pursuing the Ph.D. degree with the Chair for Integrated Systems and Photonics, Institute of Electrical Engineering and Information Technology. He is also a Scientific Staff Member with the Institute of Electrical Engineering and Information Technology. His research interests include charge carrier processes in organic semiconductor devices and the integration of nanostructures in OLEDs.



Markus Köpke was born in Hohwacht, Germany, in 1970. He received the State Certified Technician in electrical engineering from the Technical College, Kiel, in 2003. Since 2014, he has been a Technician with the Institute of Electrical Engineering and Information Technology, Kiel University. His research skills are the manufacturing of thin film layers for optoelectronic devices, fabrication of nanostructured surfaces, and development of processes in manufacturing of micro devices and characterization.



Yolande Murat received the M.S. degree in material sciences and the Ph.D. degree in physics from the University of Bordeaux, France, in 2013 and 2017, respectively.

Since 2018, she has been a Postdoctoral Researcher with the Chair for Integrated Systems and Photonics, Kiel University, Germany. Her research interests are focused on printed electronics and organic electronics, including light-emitting diodes.



Nicole Christine Schneidewind (born Klindtworth) was born in Viborg, Denmark, in 1983. She received the B.Sc. and M.Sc. degrees in engineering and mechatronics, profile in nanotechnology from the University of Southern Denmark, Sønderborg. Her research interests include production and development of matrices OLED's and OPD's and production of flexible matrices.



Martina Gerken (Member, IEEE) received the Dipl.Ing. degree in electrical engineering from the University of Karlsruhe, Germany, in 1998, and the Ph.D. degree in electrical engineering from Stanford University, Stanford, CA, USA, in 2003. From 2003 to 2008, she was an Assistant Professor with the University of Karlsruhe. In 2008, she was appointed as a Full Professor of Electrical Engineering and the Head of the Chair for Integrated Systems and Photonics, Kiel University, Germany.